

This is the accepted manuscript made available via CHORUS. The article has been published as:

Magnetic and electronic properties of $\text{CaMn}_{\{2\}}\text{Bi}_{\{2\}}$: A possible hybridization gap semiconductor

Q. D. Gibson, H. Wu, T. Liang, M. N. Ali, N. P. Ong, Q. Huang, and R. J. Cava

Phys. Rev. B **91**, 085128 — Published 27 February 2015

DOI: [10.1103/PhysRevB.91.085128](https://doi.org/10.1103/PhysRevB.91.085128)

Magnetic and Electronic Properties of CaMn_2Bi_2 , a Possible Hybridization Gap Semiconductor

Q.D.Gibson¹, H.Wu², T.Liang³, M.N.Ali¹, N.P.Ong⁴, Q.Huang², and R.J.Cava¹

¹ *Princeton University, Department of Chemistry, Princeton, NJ, 08544*

² *NIST Center for Neutron Research,*

National Institute of Standards and Technology, Gaithersburg, MD 20899-6102

³ *Department of Materials Science and Engineering,*

University of Maryland, College Park, MD 20742 and

⁴ *Princeton, University, Department of Physics, Princeton, NJ, 08544*

(Dated: December 4, 2014)

Abstract

We report the magnetic and electronic properties of CaMn_2Bi_2 , which has a structure based on a triangular-bilayer of Mn, rather than the ThCr_2Si_2 structure commonly encountered for 122 compounds in intermetallic systems. CaMn_2Bi_2 has an antiferromagnetic ground state, with a T_N of 150 K, and for a 250 K temperature range above T_N does not exhibit Curie-Weiss behavior, indicating the presence of strong magnetic correlations at high temperatures. Resistivity measurements show that CaMn_2Bi_2 exhibits semiconducting properties at low temperatures, with an energy gap of only 62 meV, indicating it to be a very narrow band gap semiconductor. The electronic structure of CaMn_2Bi_2 , examined via ab-initio electronic structure calculations, indicates that Mn 3d orbital hybridization is essential for the formation of the band gap, suggesting that CaMn_2Bi_2 may be a hybridization-gap semiconductor.

INTRODUCTION

Layered transition metal compounds are of continuing interest in materials physics, exhibiting properties such as magnetism, superconductivity[1], charge density waves [2] and extremely large magnetoresistance[3]. The discovery of superconductivity in layered Fe-Se and Fe-As compounds[4–6] has revived interest in the layered Mn-pnictides. With the recent discoveries of BaMn_2Bi_2 [7] and BaMnBiF [8] for example, Mn-Bi compounds have emerged as interesting analogs to the Fe based superconductors; they are expected to have lower band gaps and have easier accessible metallicity than other Mn pnictides due to the presence of the Bi layers. Here we report the electronic and magnetic properties of single crystals of hexagonal CaMn_2Bi_2 , which exhibits unusual magnetism and a small band gap, with semiconducting transport properties. Further, through electronic structure calculations, we show that the hybridization of the Mn 3d orbital electronic states is important for imparting the semiconducting properties. From this we infer that CaMn_2Bi_2 is a candidate material for a hybridization gap semiconductor, in which localized states (such as d or f states) hybridize with a metallic band structure and form a band gap, such as in $\text{Ce}_3\text{Bi}_4\text{Pt}_3$ [9] .

EXPERIMENTAL

CaMn_2Bi_2 single crystals were grown using a Bi flux method[10]. Magnetic susceptibility, resistivity, and temperature dependent hall and heat capacity measurements were taken on single crystal samples using a Quantum Design Physical Properties Measurement System. Single crystals of mass 42mg and 18mg were used for the susceptibility and heat capacity measurements, respectively. A crystal cut into a bar of dimensions 1x1x2 mm was used for transport measurements. Measurements of magnetization vs. applied magnetic field were linear above the magnetic ordering transition to applied fields of $\mu_0 H = 1.0$ Tesla, and thus magnetic susceptibility is defined as $\chi = M/H$, where M is the measured magnetization in that field. The field dependent Hall measurement was performed using a Keithley current sourcemeter and voltmeter. The orientation of the crystals for the single crystal transport and magnetic measurements was determined by single crystal x-ray diffraction. The natural facets were shown to be the 011 and 201 crystal faces. All transport data were taken within the (011) plane. The more intuitive [001] and [100] crystallographic directions could not be

measured due to a lack of well defined facets corresponding to those directions.

Neutron powder diffraction (NPD) data were collected at the NIST Center for Neutron Research on the high resolution powder neutron diffractometer for various temperatures from 5 K to 295 K to elucidate the possible magnetic and crystal structure transitions. The temperature dependence of the peak intensity at the (100) magnetic reflection was monitored on warming to characterize the magnetic transition[11].

Electronic structure calculations were performed in the framework of density functional theory using the Wien2k code [12] with a full-potential linearized augmented plane-wave and local orbitals basis together with the Perdew-Burke-Ernzerhof parameterization of the generalized gradient approximation [13]. The plane wave cutoff parameter $R_{MT}K_{max}$ was set to 7 and the Brillouin zone (BZ) was sampled by 2000 k-points. LDA+U calculations were also performed, with $U_{eff}=U-J$. Spin orbit coupling was included. The calculations were all performed with spin-polarization, using the experimental antiferromagnetic configuration.

RESULTS AND DISCUSSION

CaMn_2Bi_2 has a hexagonal structure (Figure 1a)[14], related to the ThCr_2Si_2 structure found for the iron arsenide superconductors, as it is composed of layers of Metal-Pnictide tetrahedra separated by alkaline earth layers. The primary difference is in the geometry of the transition metal layers - in CaMn_2Bi_2 , the Mn-bilayer can be considered as a puckered Mn honeycomb, while in ThCr_2Si_2 -type compounds such as BaFe_2As_2 , the Fe plane is a simple square net.

The temperature dependent magnetic susceptibility for CaMn_2Bi_2 between 5 and 400 K is shown in Figure 1(b). The susceptibility is almost temperature independent in the 400–150 K temperature range, with a broad weak peak that appears to be centered around 300K. The susceptibility decreases quickly after a distinct change in slope on cooling below 150K due to the presence of a magnetic phase transition, as confirmed by further measurements. Upon further cooling, the susceptibility levels off and then increases again at low temperatures. The low temperature increase is possibly due the presence of paramagnetic impurities (such as Mn^{2+} ions occurring as defects); the low temperature behavior was sample dependent, while the higher temperature behavior was consistent across all samples. However the low temperature behavior being intrinsic cannot be completely ruled out. Figure 1(b) inset shows

the magnetization versus applied field (MH) curves at 30K, 200K and 300K. The 300K and 200K curves are linear for the whole field range up to 9 T. The 30K curve, however, which is well below the magnetic ordering transition temperature, shows a slight field dependence, indicating that there may be some field induced spin canting or other mechanism disturbing the spontaneously ordered Mn moments in applied fields in the 2 Tesla or greater range.

Figure 2(a) shows the observed powder neutron diffraction pattern of CaMn_2Bi_2 at 5 K. The fitted curve includes both the refined crystal structure and magnetic structure models, indicating that both are well understood. The counts for the (100) diffraction peak, which is a magnetic diffraction peak, as a function of temperature, are shown in figure 3(a-inset). This shows that the three-dimensional magnetic ordering begins at 154 K, consistent with the magnetic susceptibility measurements. The ordering transition follows a typical mean field behavior, with I^2 going as $(T_N - T)$. The 100 peak is shown to grow into the diffraction pattern in Figure 2(b).

The magnetic ground state is antiferromagnetic (AFM), as shown in Figure 2(c), with an ordered Mn moment at 5 K of $3.85\mu_B$, which is similar to that found in related systems [15–17]. The arrangement of Mn (or the magnetic structure) can be described using a Shubnikov magnetic space group of $P-1'$ with opposite magnetic moments alternating between the nearest neighboring Mn atoms. The nearest neighbor Mn atoms in the bilayer have opposing spins; when considered as a puckered Mn honeycomb lattice, this alternating spin orientation ordering is a typical Neel state for honeycombs. Considered as Mn "bilayers", the coupling between neighboring bilayers is ferromagnetic, resulting in the magnetic unit cell being the same size as the nonmagnetic cell (though with a magnetic symmetry that allows the 100 reflection). This is the same type of antiferromagnetic ordering observed in similar systems such as CaMn_2Sb_2 and BaMn_2Bi_2 [15, 16], i.e. nearest neighbor Mn atoms in-plane having opposite spins.

The phase transition at around 150K was further studied by heat capacity measurements (Figure 2(d)). These measurements show a well-defined peak at around 150 K; no further phase transitions were observed in the 2-300K temperature range. While the T_N as derived from the neutron scattering appears to be higher than the temperature of the peak in the heat capacity, it is consistent with when the heat capacity appears to diverge from expected behavior; the T_N is labelled on the figure. However, as there is no good non-magnetic structural analogue for CaMn_2Bi_2 , the phonon contribution to the specific heat

cannot be rigorously subtracted. The fact that the susceptibility in such a highly magnetic system is approximately temperature independent between 150 and 400 K, a range of about 250K above the AFM ordering temperature, implies that local AFM correlations are very strong well above T_N ; the magnetic moments are very likely short range ordered for a very wide range of temperature above T_N . In fact, the susceptibility bears some resemblance to a model of itinerant spin density wave (SDW) magnetism with a very small density of states[18]. Future work, including measuring other crystallographic directions, may reveal the nature of the magnetic behavior above T_N .

To further characterize the properties of CaMn_2Bi_2 , resistivity and Hall effect measurements were performed. Figure 3(a) shows the resistivity behavior of a representative single crystal sample of CaMn_2Bi_2 . CaMn_2Bi_2 crystals consistently exhibit "metallic" resistivity (resistivity that decreases with decreasing temperature) behavior between about 300K and 70K, with a kink at 150K due to the AFM transition. Below about 70K, the resistivity shows activated behavior, and then levels off at a maximum value that is sample dependent. This leveling off of the resistivity could be due to either impurity or surface state conduction (see below).

The field and temperature dependent Hall resistivity curves for the samples in figure 3(a) are shown in Figure 3(b). The curves show p-type behavior and are linear in field through a large temperature range. Below about 40 K, however, the Hall resistivity vs. applied field curves become highly nonlinear, an indication of the presence of two carrier types. At low temperatures, consistent with the leveling off of the resistivity, the hall resistivity becomes linear again, and very small.

In order to understand the higher temperature "metallic" behavior of CaMn_2Bi_2 , the temperature dependence of the resistivity and Hall resistivity were taken for another representative sample. The log resistivity vs. $1/T$ plot for this sample is shown in Figure 4 (upper panel). This figure shows the development of activated behavior, with $\frac{E_a}{k_b} = 11\text{meV}$ in the 20-50K temperature range. In contrast with the resistivity, the Hall resistivity (Figure 4a, lower panel) shows activated behavior over the entire temperature range and does not change much through the AFM transition. This suggests that the AFM transition does not substantially affect the carrier concentration or Fermi surface, but instead primarily changes the carrier mobility likely due to decreased magnetic scattering. This indicates that the transport behavior is in the activated regime and that CaMn_2Bi_2 is semiconducting at

all temperatures investigated, and that the "metallic" like resistivity is due to a strongly temperature dependent mobility rather than actual metallic behavior.

The $\log R_H$ vs. $1/T$ plot is shown in the inset. Two regimes are observed, at high and low temperatures, with different activation energies. The low temperature activation energy is consistent with the one derived from the resistivity. The high temperature activation energy is larger, however, and likely related to the intrinsic band gap of the material. From the resistivity and hall data, the nominal hall mobility was calculated from 300K to 40K (Figure 4b; lower panel inset), assuming one carrier type. (Because the Hall response becomes nonlinear below about 40K, data is not shown below that temperature.) While there are likely both holes and electrons present even in the higher temperature regime, this data was used as an approximation, in order to understand the temperature dependence of the resistivity. The analysis shows that the nominal mobility increases upon cooling. A kink in the mobility is seen at the AFM transition. The mobility then increases dramatically before leveling off in the 40-50 K regime. CaMn_2Bi_2 therefore shows activated behavior throughout the entire temperature range; the "metallic" conductivity at high temperature is due to an increase in carrier mobility with temperature that is a stronger effect than the decrease in carrier concentration with temperature. A fit to the low temperature heat capacity (Figure 4c) gives a Sommerfield coefficient γ within error of 0, confirming the presence of very few charge carriers in the system at low temperatures. The low temperature resistivity and activation energy are both significantly smaller than the closest analogous compounds, CaMn_2Sb_2 and BaMn_2Bi_2 [19, 20]. The resistivity is also consistent with the heat capacity; a large peak in the temperature derivative of the resistivity is seen near T_N (Figure 4d); again T_N is consistent with where the derivative begins to diverge from expected behavior. We note that the derivative of $X(T)*T$ with respect to T shows a similar temperature dependence. However, due to very the small variation in $X(T)$ in the 150-300K region, this derivative is noisy and is not shown.

In order to understand the semiconducting behavior of CaMn_2Bi_2 , electronic structure calculations were performed that included the experimentally determined AFM ordered state of the Mn. The electronic band structure is shown in Figure 6(a), with the contributions of the Mn and Bi states plotted heavier (left to right, respectively). The calculations show that the conduction band near E_F consists primarily of relatively non-dispersive Mn 3d states, with one dispersive Bi(s)-Mn(s) hybrid band cutting through them to the bottom of the

conduction band. The Bi(s)-Mn(s) band refers to the fact that this band derives mainly from both Mn s and Bi s orbitals, indicating that the unoccupied Mn s states are strongly hybridized with the occupied Bi s orbitals. In contrast, the valence bands are composed of Mn (3d) -Bi(p) hybrid states. This calculation show a slight energy overlap between the valence band and conduction band states due to the usual DFT underestimation of the band gap, but the distinction between valance band and conduction band states is clear.

Figure 6(b) shows the calculated spin up density of states (DOS). (The spin down density of states is the same, with the Mn(1) and Mn(2) labels switched.) The DOS shows that essentially localized AFM ordered Mn d electron states - the E vs. k behavior shows that bands are only weakly dispersive - are found just above E_F and also at about 3 eV below E_F . There is also significant Mn d contribution in the valence band below E_F , from both spin up and spin down Mn atoms, at energies from 0 to -3 eV with respect to E_F . This second Mn contribution to the DOS in the valence band is representative of delocalized electrons, and the degeneracy of the Mn(1) and Mn(2) contributions means they are not impacted by the AFM ordering; the strongly hybridized Mn d states in the valence band are an important and large contribution. The calculated moment per Mn is $4.13 \mu_B$ per Mn, which is very close to the observed ordered value. Thus both the experiment and the calculation imply that approximately one d electron per Mn atom is delocalized and hybridized with the Bi p states in the valence band, while the others are localized, giving rise to the observed large magnetic moment.

To illustrate what we propose is the overall electronic picture for CaMn_2Bi_2 , a cartoon schematic of its calculated electronic structure is shown in Figure 6(a). In order to understand the importance of the Mn d orbital hybridization on this electronic structure, additional calculations were performed with volume expanded and volume contracted lattices (Fig 6(b)). Upon lattice compression, the gap between the valence band and the Bi-Mn s hybrid band above E_F becomes larger, while the indirect gap between the Mn d states in the conduction band and the valence band becomes very slightly smaller. Conversely, upon lattice expansion, the gap between the valence band and the Bi-Mn s derived conduction band decreases, even going through a metallic state at $V=1.1V_0$. This is contrary to the normal behavior of materials, where compression of cell volumes increases the electronic hybridization and therefore decreases band gaps; here the opposite is found.

Similarly anomalous results were obtained by adding a coulomb repulsion term "U" to

the Mn 3d states in the calculation. Under normal circumstances the addition of the U term is expected to push d electron states away from E_F and prevent hybridization. Adding a U term in this case does indeed have the effect of moving the 3d states away from E_F but also, in contrast, it closes the gap between the top of the valence band and the Bi-Mn s band above E_F . By $U_{eff} = 7\text{eV}$, a zero band gap state is calculated. That the calculated lattice expansion and coulomb repulsion effects are similar indicates that it is the hybridization of the Mn 3d orbitals that results in the very small band gap in CaMn_2Bi_2 . The calculations imply that the hybridization of the Mn 3d states is actually required to make the compound semiconducting, as there is no gap when the hybridization is turned off, either by "U" or by lattice expansion. This behavior is not expected for the usual semiconductor, but this exact mechanism of hybridization of localized states giving rise to a band gap is the proposed mechanism for all hybridization gap insulators, such as Ce based compounds like $\text{Ce}_3\text{Bi}_4\text{Pt}_3$ [9] and for the Fe 3d based compound FeSi [21, 22]. Given this, we infer that CaMn_2Bi_2 can be classified as an excellent candidate of a correlated hybridization gap semiconductor. The fact that strong Mn 3d-pnictide hybridization helps to open a band gap in this material may provide a generic reason why Mn pnictides tend to be insulators, while Fe pnictides tend to be metals or semi-metals.

CONCLUSIONS

We report the magnetic and electronic properties of hexagonal layered CaMn_2Bi_2 . This material was found to display antiferromagnetic ordering with a T_N of 150 K along with strong antiferromagnetic suppression of the susceptibility, implying low dimensional antiferromagnetic ordering, for a temperature range of at least 250 K above T_N . Furthermore, CaMn_2Bi_2 is a narrow gap semiconductor, with a strong temperature dependence of the nominal hall mobility which leads to an apparent metallic resistivity. The high temperature transport gap is 62 meV while the low temperature gap is only around 12 meV. Band structure calculations indicate that Mn 3d orbital hybridization is key to opening the band gap, and that localized or quasi-localized Mn 3d orbitals dominate the conduction band just above E_F . We thus infer that CaMn_2Bi_2 is a correlated, antiferromagnetic, hybridization gap semiconductor. Further study into this or similar systems may elucidate the relationship between the correlated antiferromagnetic state of Mn and Fe pnictides and the supercon-

ductivity observed in Fe-As and Fe-Se compounds.

ACKNOWLEDGMENTS

Q.D.G, M.N.Ali and R.JC acknowledge support from SPAWAR grant (NN6601-11-1-4110) and the AFOSR MURI grant (FA9550-09-1-0953) N.P.O. and T.L. are supported by the Army Research Office (ARO W911NF-11-1-0379) and the National Science Foundation (grant number DMR 0819860). T.L acknowledges scholarship support from the Japan Student Services Organization. We acknowledge helpful discussions with M.K.Fuccillo and N.Haldolarachchige.

-
- [1] E. Morosan, H. Zandbergen, B. Dennis, J. Bos, Y. Onose, T. Klimczuk, A. Ramirez, N. Ong, and R. Cava, *Nature Physics* **2**, 544 (2006).
 - [2] G. Li, W. Hu, D. Qian, D. Hsieh, M. Hasan, E. Morosan, R. Cava, and N. Wang, *Physical review letters* **99**, 027404 (2007).
 - [3] M. N. Ali, J. Xiong, S. Flynn, Q. Gibson, L. Schoop, N. Haldolaarachchige, N. Ong, J. Tao, and R. Cava, *arXiv preprint arXiv:1405.0973* (2014).
 - [4] X. Wang, Q. Liu, Y. Lv, W. Gao, L. Yang, R. Yu, F. Li, and C. Jin, *Solid State Communications* **148**, 538 (2008).
 - [5] M. Rotter, M. Tegel, and D. Johrendt, *Physical Review Letters* **101**, 107006 (2008).
 - [6] F.-C. Hsu, J.-Y. Luo, K.-W. Yeh, T.-K. Chen, T.-W. Huang, P. M. Wu, Y.-C. Lee, Y.-L. Huang, Y.-Y. Chu, D.-C. Yan, *et al.*, *Proceedings of the National Academy of Sciences* **105**, 14262 (2008).
 - [7] B. Saparov and A. S. Sefat, *Journal of Solid State Chemistry* **204**, 32 (2013).
 - [8] B. Saparov, D. J. Singh, V. O. Garlea, and A. S. Sefat, *Scientific reports* **3** (2013).
 - [9] M. F. Hundley, P. C. Canfield, J. D. Thompson, Z. Fisk, and J. M. Lawrence, *Phys. Rev. B* **42**, 6842 (1990).
 - [10] Crystals were grown from elemental starting materials in the ratio $\text{CaMn}_2\text{Bi}_{10}$. The elements were sealed in an evacuated quartz ampoule, and heated to 1000 C at 3C/min. The ampoule was held at 1000C for two days and then cooled to 400C at 0.1C/min and was centrifuged

- while hot to decant the excess Bi. ().
- [11] Neutron diffraction measurements performed on diffractometer BT1, with monochromatic neutrons of wavelength 2.0775 Å produced by a Ge(311) monochromator. Soller collimations before and after the monochromator and after the sample were 60, 20, and 7 minutes full-width-at-half-maximum (FWHM), respectively. The diffraction measurements were taken on ground single crystals. Data were collected in the 2θ range of 3 deg to 168 deg with a step size of 0.05 degree. Refinements of the nuclear and magnetic structures were carried out using the neutron powder diffraction data and the program GSAS (A. C. Larson, R. B. Von Dreele, Los Alamos National Laboratory Report No. LAUR086-748 (1990)). The neutron scattering amplitudes employed were 0.490, -0.373, and 0.853 cm⁻¹² for Ca, Mn, and Bi, respectively. ().
 - [12] P. Blaha, K. Schwarz, P. Sorantin, and S. Trickey, Computer Physics Communications **59**, 399 (1990).
 - [13] J. Perdew, K. Burke, and M. Ernzerhof, Physical review letters **77**, 3865 (1996).
 - [14] G. Cordier and H. Schäfer, Z. Naturforsch. B , 1459 (1976).
 - [15] W. R. II, A. L. Sharma, A. Gomes, J. Gonzalez, Q. Huang, and J. Singleton, Journal of Magnetism and Magnetic Materials **321**, 2612 (2009).
 - [16] S. Calder, B. Sapiro, H. Cao, J. Niedziela, M. Lumsden, A. Sefat, and A. Christianson, arXiv preprint arXiv:1310.7317 (2013).
 - [17] A. Beleanu, J. Kiss, G. Kreiner, C. Köhler, L. Muehler, W. Schnelle, U. Burkhardt, S. Chadov, S. Medvedev, D. Ebke, *et al.*, Physical Review B **88**, 184429 (2013).
 - [18] M. Korshunov, I. Eremin, D. Efremov, D. Maslov, and A. Chubukov, Physical review letters **102**, 236403 (2009).
 - [19] K. Wang and C. Petrovic, Applied Physics Letters **103**, 192104 (2013).
 - [20] J. W. Simonson, G. J. Smith, K. Post, M. Pezzoli, J. J. Kistner-Morris, D. E. McNally, J. E. Hassinger, C. S. Nelson, G. Kotliar, D. N. Basov, and M. C. Aronson, Phys. Rev. B **86**, 184430 (2012).
 - [21] Z. Schlesinger, Z. Fisk, H.-T. Zhang, M. Maple, J. DiTusa, and G. Aeppli, Physical review letters **71**, 1748 (1993).
 - [22] C. Fu, M. Krijn, and S. Doniach, Physical Review B **49**, 2219 (1994).

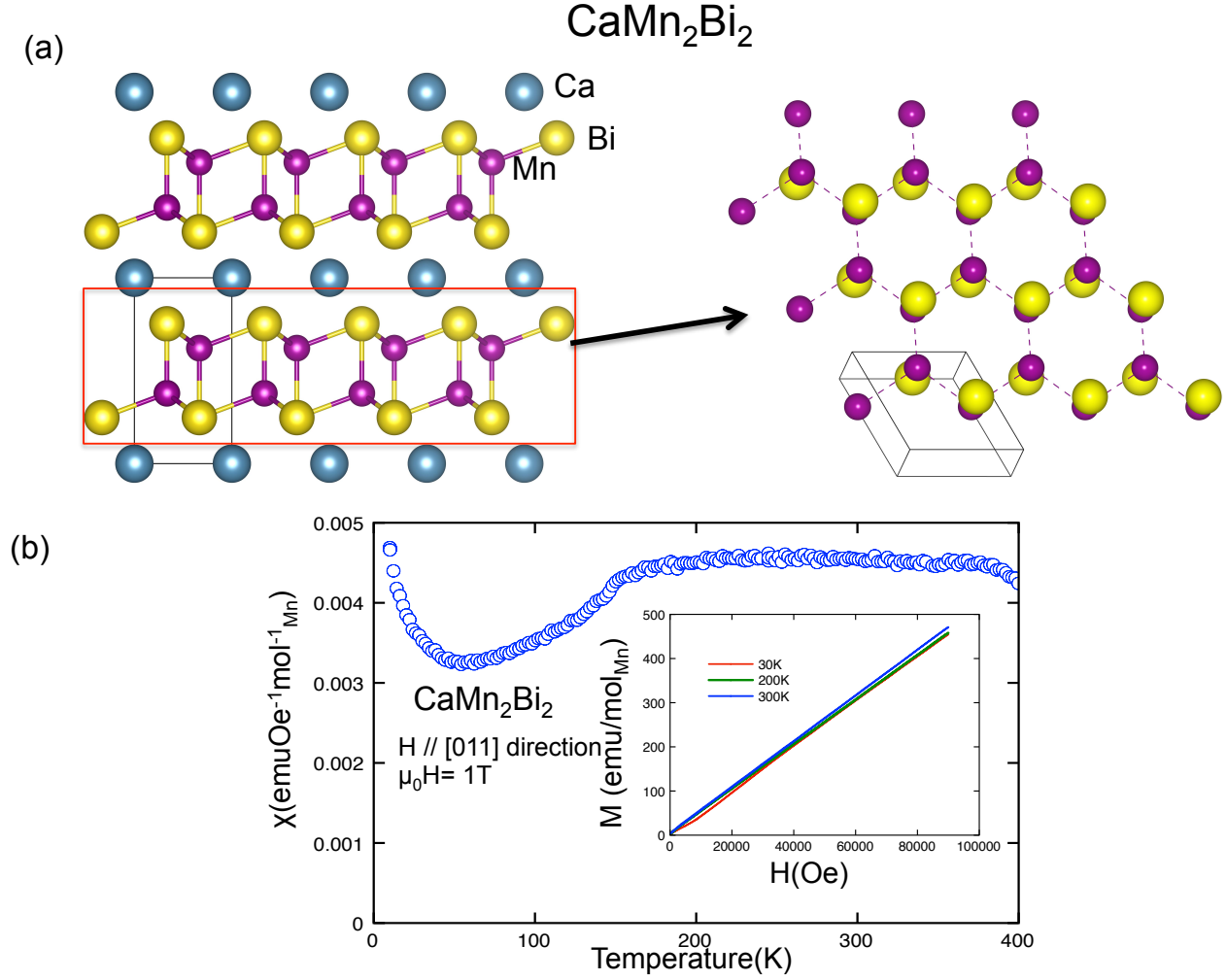


FIG. 1. (a) The crystal structure of CaMn_2Bi_2 (left), and a top-down view of the Mn-Bi hexagonal sub lattice (right). (b) Magnetic susceptibility versus temperature taken with $\mu_0 H = 1\text{T}$. Inset: Magnetization versus applied field curve for three different temperatures.

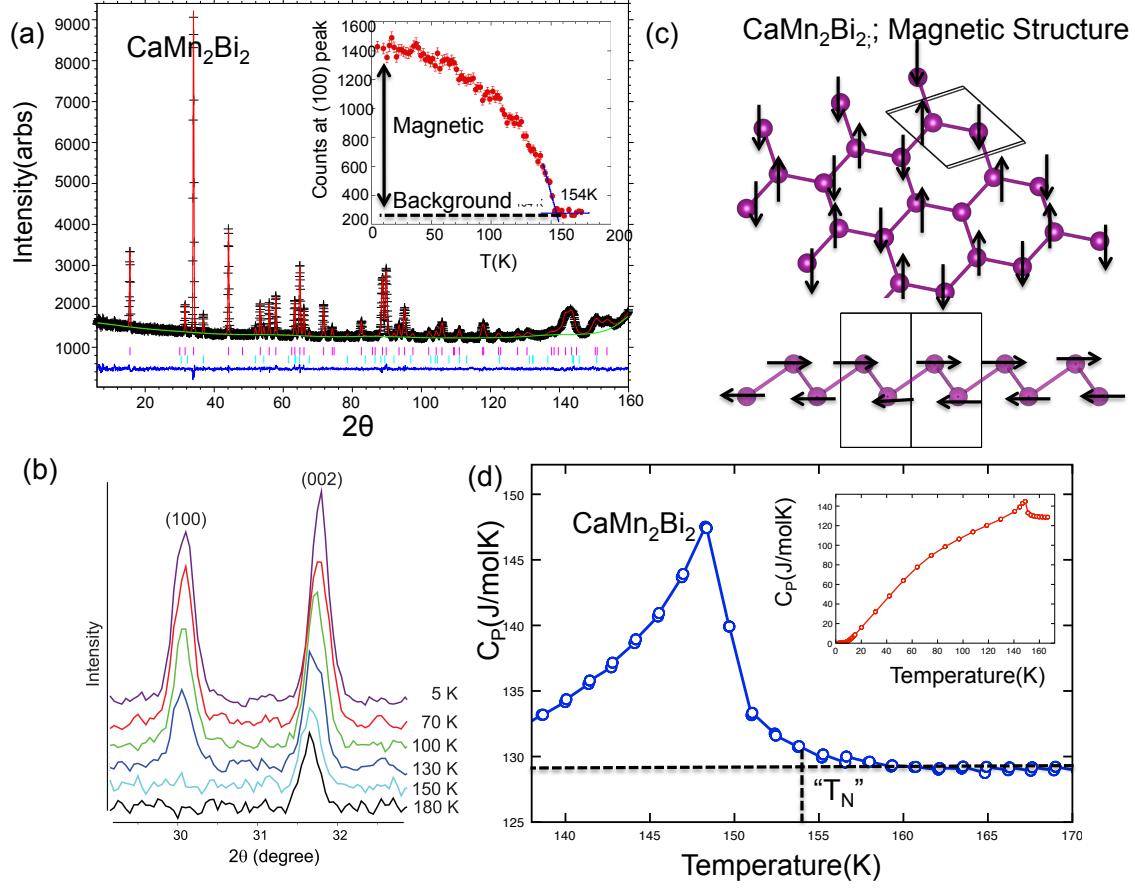


FIG. 2. (a) Neutron diffraction pattern with the refined cell pattern overlaid. Inset: Counts of the (100) peak as a function of temperature, showing the transition temperature. (b) A plot of the intensity of the diffraction peaks at various temperatures, showing the growing in of the magnetic diffraction peak with temperature. (c) Two views of the magnetic structure of CaMn_2Bi_2 showing the spins alternating between nearest neighbor Mn atoms. Top: the Mn moment ordering from an overview of the puckered honeycomb sub lattice. Bottom: a side view of the Mn sub lattice. (d) Heat capacity versus temperature, showing the peak due to the AFM transition. The T_N as derived from neutron scattering is labeled. Inset: Heat capacity over a wider temperature range.

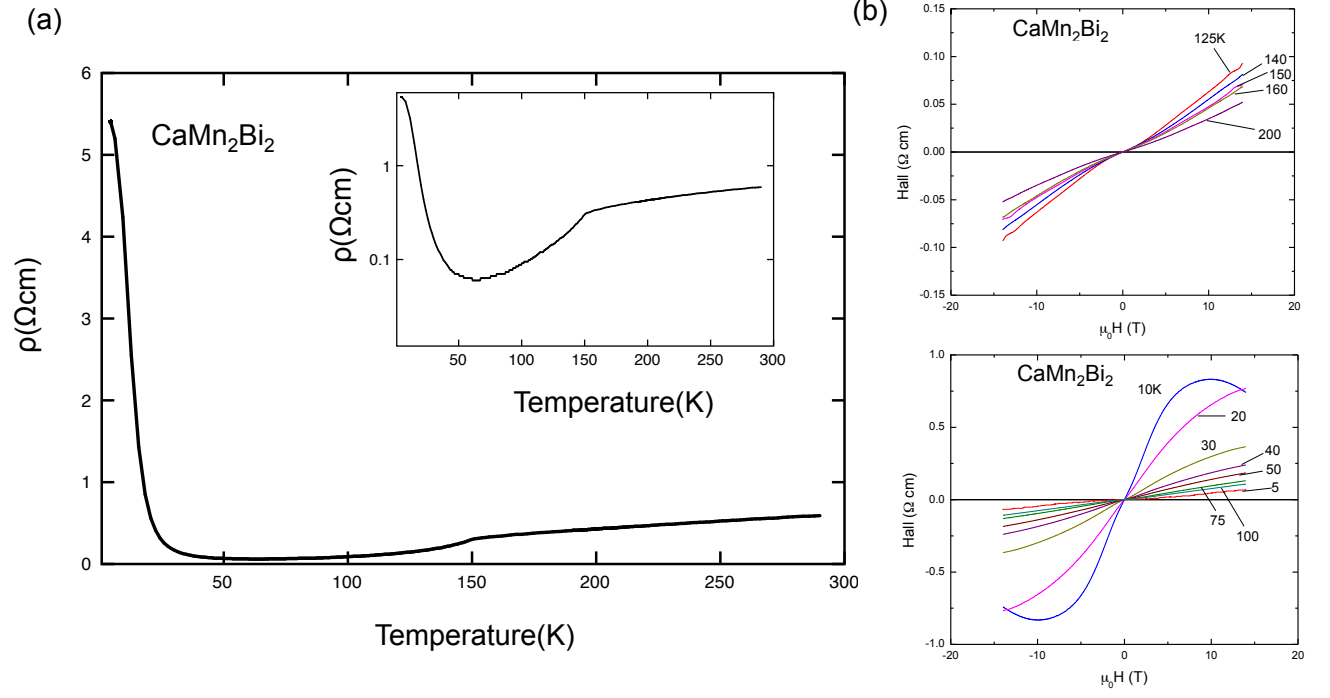


FIG. 3. (a) Resistivity versus temperature for a representative single crystalline sample. A log scale is inset for clarity. (b) Hall resistivity versus field curves at various temperature for a representative sample.

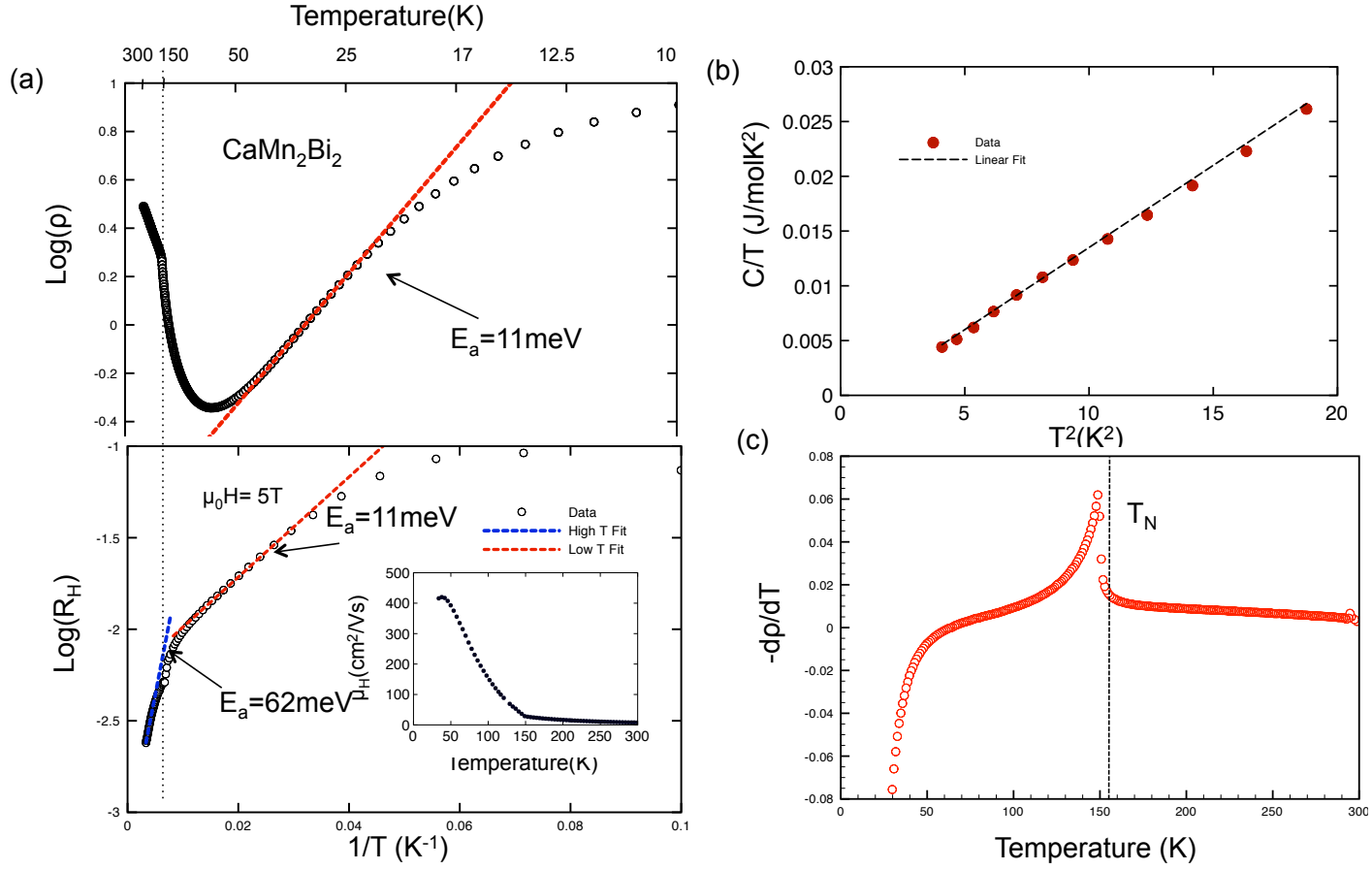


FIG. 4. (a) A plot of the log of resistivity versus reciprocal temperature (top). The red dashed line is a linear fit, showing activated behavior. Bottom: a plot of the log of hall resistivity versus temperature, showing activated behavior with two regions. The blue line and red line are linear fits in the high temperature region and low temperature region, respectively. Inset: the nominal Hall mobility versus temperature. (b) A linear fit to C/T vs. T^2 . (c) A plot of $(-dp/dT)$ vs. T showing a qualitative agreement with the heat capacity; the T_N is labelled.

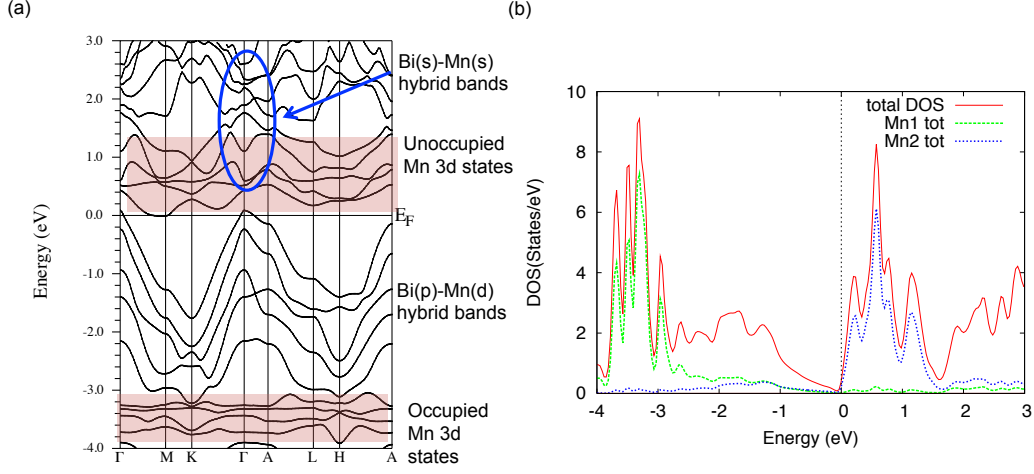


FIG. 5. (a) Electronic band structure of AFM CaMn_2Bi_2 . The AFM ordered Mn 3d states are highlighted in red, and states from the Bi-Mn s hybrid band are circled in blue. (b) The spin-up Density of states (DOS) plot also showing the partial DOS of the Mn(1) and Mn(2) d states.

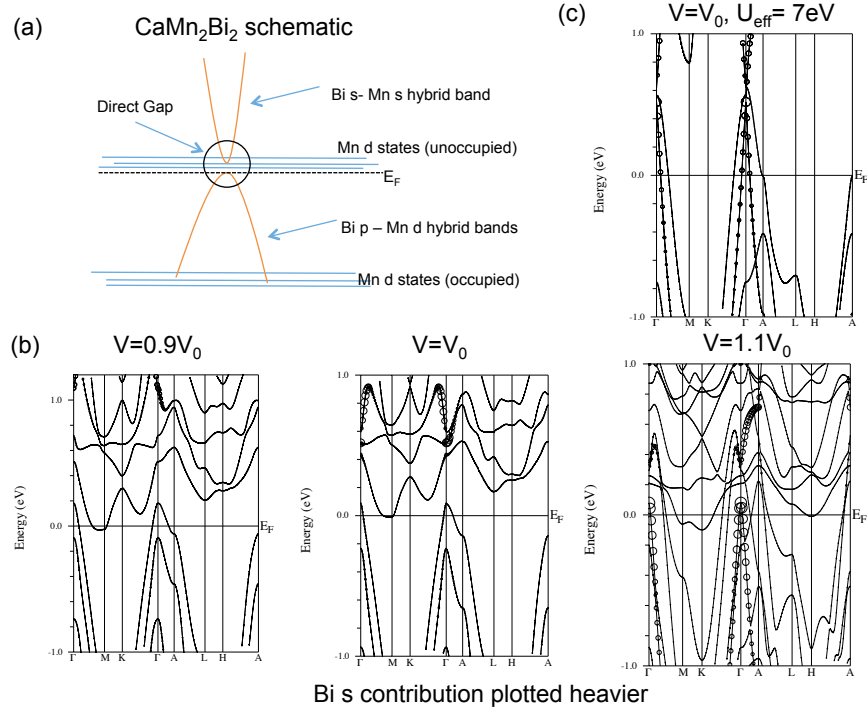


FIG. 6. (a) Cartoon schematic of the electronic structure of CaMn_2Bi_2 . (b) The band structure of CaMn_2Bi_2 at various volumes, with the Bi s states plotted heavier. Left to right: $0.9V_0$, V_0 and $1.1V_0$. (c) The band structure of the metallic state with $U_{\text{eff}}=7\text{eV}$.